Biochar

ORIGINAL RESEARCH

Biochar-induced alterations in *Acidithiobacillus ferrooxidans* activity and its impact on Cd(II) and As(III) adsorption from acid mine drainage

Peng Fu[1], Fangling Chang[1], Dongxu Yuan[1], Yanyan Wang[2], Yingxuan Fan[1], Yufan Kang[1], Lixiang Zhou[3], Chen Yang[1], Wenlong Bi[1], Junmei Qin[1], Hong Yang[4] and Fenwu Liu[1*]

Abstract

Due to continuing mining activities, Cd(II) and As(III) contamination in acid mine drainage (AMD) has become a major environmental challenge. Currently, there is increasing focus on the use of biochar to mitigate AMD pollution. However, the impact of biochar on the process of Fe(II) oxidation by *Acidithiobacillus ferrooxidans* (*A. ferrooxidans*) in AMD systems has not been determined. In this study, we investigated the effects of introducing biochar and biochar-leachate on Fe(II) biooxidation by *A. ferrooxidans* and on the removal of Cd(II) and As(III) from an AMD system. The results showed that the biochar-leachate had a promoting effect on Fe(II) biooxidation by *A. ferrooxidans*. Conversely, biochar inhibited this process, and the inhibition increased with increasing biochar dose. Under both conditions (c(*A. ferrooxidans*) = 1.4×10^7 copies mL^{-1}, m(FeSO$_4$·7H$_2$O):m(biochar) = 20:1; c(*A. ferrooxidans*) = 7.0×10^7 copies mL^{-1}, m(FeSO$_4$·7H$_2$O):m(biochar) = 5:1), the biooxidation capacity of *A. ferrooxidans* was severely inhibited, with Fe(II) oxidation efficiency reaching a value of only ~ 20% after 84 h. The results confirmed that this inhibition might have occurred because a large fraction of the *A. ferrooxidans* present in the system adsorbed to the biochar, which weakened bacterial activity. In addition, mineral characterization analysis showed that the introduction of biochar changed the *A. ferrooxidans* biooxidation products from schwertmannite to jarosite, and the specific surface area increased after the minerals combined with biochar. Coprecipitation experiments of As(III) and Cd(II) showed that Cd(II) was adsorbed by the biochar over the first 12 h of reaction, with a removal efficiency of ~ 26%. As(III) was adsorbed by the generated schwertmannite over 24 h, with a removal efficiency of ~ 100%. These findings have positive implications for the removal of As(III) and Cd(II) from AMD.

Highlights

- Biochar-leachate promoted Fe(II) biooxidation by *A. ferrooxidans*.
- Biochar inhibited *A. ferrooxidans*-mediated schwertmannite formation by adsorption.
- Cd(II) was adsorbed by biochar during the initial reaction stage.
- As(III) was adsorbed by schwertmannite that is gradually generated in the AMD system.

Graphical Abstract

1 Introduction

The industrial sector contributes substantially to global environmental pollution, and acid mine drainage (AMD) from mining activities has become a widespread environmental concern worldwide (Yang et al. 2013, 2012). AMD is a special type of wastewater that is primarily produced in high-Fe and high-S mining areas through the oxidation of minerals with oxygen in air or water (Tu et al. 2022; Valente et al. 2015). Because of the large amount of H^+ generated during the reaction process, AMD is strongly acidic, with a pH generally less than 4. Moreover, because sulfur-bearing minerals are often accompanied by various trace elements, AMD contains high concentrations of metal/metalloid (e.g., Cd and As) and sulfates, which are extremely harmful to the environment (Du et al. 2022; Masindi et al. 2022). The total length of AMD-polluted rivers worldwide exceeds 23,000 km, approximately 16,000 km of which are affected by severe pollution, causing substantial damage to global ecosystems (Chen et al. 2021; Wang et al. 2020). Additionally, in recent years in some developing countries such as China, many abandoned open-cast coal mines have been left unmanaged,

causing serious damage to local water resources and aqueous environments (Park et al. 2019). Moreover, the indiscriminate discharge of AMD destroys soil structure, leading to soil acidification and damaging the growing environment of plants and animals, thereby reducing food production and posing a threat to the natural environment and human society.

The process of AMD formation involves the oxidation of sulfur-bearing minerals via processes such as chemical and biological oxidation, among which biological oxidation plays a key role (Jiao et al. 2023). Several acidophilic microorganisms, such as *Acidithiobacillus ferrooxidans* (*A. ferrooxidans*), are widely found in AMD. *A. ferrooxidans* is a bacterium that was first isolated from AMD by Colmer and Hinkle (1947). It is a gram-negative, aerobic, acidophilic, obligate chemolithoautotrophic bacterium (Zhan et al. 2019). It grows fastest in 9 K liquid media ($FeSO_4 \cdot 7H_2O$: 44.2 g L^{-1}, KCl: 0.119 g L^{-1}, K_2HPO_4: 0.058 g L^{-1}, $MgSO_4 \cdot 7H_2O$: 0.583 g L^{-1}, $(NH_4)_2SO_4$: 3.5 g L^{-1}, $Ca(NO_3)_2 \cdot 4H_2O$: 0.0168 g L^{-1}) at 28–30 °C and pH = 2.5 (Liu et al. 2020; Yue et al. 2023). *A. ferrooxidans* is widely found in various environments

including soil, seawater, volcanic ash, AMD, and acidic environments containing Fe or S (Zhan et al. 2019). It can obtain electrons and energy for growth and reproduction by oxidizing Fe(II) and reducing inorganic sulfur for the fixation of CO_2 and nitrogen (Moinier et al. 2017). Generally, in an acidic environment (pH < 4.5), the chemical oxidation rate of Fe(II) is slow. However, the biological oxidation rate catalyzed by *A. ferrooxidans* is approximately 10^2–10^6 times greater than that of chemical oxidation. In addition, Fe(III) produced by oxidation is capable of accelerating the oxidation of sulfides. The oxidation rate of sulfides by Fe(III) is 10–100 times higher than that of O_2 when the pH < 3 (Jiao et al. 2023). These processes further acidify water bodies, greatly contributing to the formation of AMD and making it a persistent form of pollution that is extremely difficult to treat (Pierre Louis et al. 2015; Zhao et al. 2015). With the continuous development of the mining industry in modern society, AMD has become a major challenge for the global mining sector and a popular and difficult issue in current environmental management.

In recent years, researchers have developed several techniques to control AMD contamination based on AMD characteristics. Adsorption has received extensive attention in the field of metal/metalloid removal owing to its low cost, high efficiency, and environmental friendliness (Anawar et al. 2015; Du et al. 2022). Secondary iron minerals (such as schwertmannite) generated via the oxidation of Fe(II) by *A. ferrooxidans*, which are abundant in AMD, can effectively remove metalloids such as As, with an adsorption capacity reaching 113.9 mg g^{-1} for As(III) (Liao et al. 2011). In addition, among the various adsorbent materials, biochar has abundant surface-active functional groups, a high specific surface area, a unique pore structure, and stable chemical properties. Therefore, these materials have strong potential for adsorbing and fixing heavy metals and improving environmental quality. As an environmentally friendly material, biochar has been widely used to remove various heavy metals from wastewater (Duan et al. 2020; Islam et al. 2021; Qiu et al. 2021). Studies have shown that the Cd(II) adsorption capacity of corn straw biochar can reach a value of 38.91 mg g^{-1} (Chi et al. 2017).

Increasing attention is being given to the application of biochar to remediate environmental pollution (Xi et al. 2022; Yang et al. 2015). However, the introduction of biochar affects the growth, reproduction, and ability of *A. ferrooxidans* to biooxidize Fe(II), and these issues warrant further investigation. Studies have shown that biochar can provide attachment surfaces and nutrients for microorganisms and promote electron transfer as an electron medium (Dong et al. 2022). Studies have also confirmed that biochar can adsorb large amounts

of Fe(II) and *A. ferrooxidans* from systems and increase system pH, thus inhibiting the dissolution of chalcopyrite and the formation of AMD (Yang et al. 2020a). Moreover, our previous study showed that the introduction of biochar significantly inhibited the ability of *A. ferrooxidans* to biooxidize Fe(II) (Fu et al. 2023).

Therefore, in the present study, we investigated and verified the role of biochar in the *A. ferrooxidans*-driven biooxidation of Fe(II) on the basis of previous studies. The main objectives of this study were to (1) investigate the effects of biochar and biochar-leachate on the *A. ferrooxidans* biooxidation process by adjusting the density of *A. ferrooxidans* and the dose of biochar and biochar-leachate; (2) analyze the changes that occur in the biooxidation products of *A. ferrooxidans* after biochar is introduced via material characterization; and (3) investigate the effect of biochar introduction into the AMD system on heavy metal (Cd(II)) and metalloid (As(III)) removal. In this study, we explored the combined potential of environmentally friendly materials and microorganisms to treat AMD, demonstrated the impact of the introduction of biochar into AMD systems and provided innovative solutions for the removal of metals/metalloids from AMD.

2 Materials and methods
2.1 Preparation of experimental materials

Preparation of biochar (BC): According to methods in our previous study (Fu et al. 2023), first, a ceramic crucible was filled with crushed corn straw (particle size < 1 mm), the straw was compacted, and the crucible was sealed with a lid to prevent the entry of oxygen. Then, the crucible was placed in a muffle furnace (LX0711, Tianjin, China) for pyrolysis under oxygen-limited conditions. The temperature of the furnace was increased to 500 °C at a rate of 5 °C min^{-1} and maintained for 3 h. After pyrolysis, the crucible was cooled to room temperature, after which the corn straw biochar (BC) was collected and stored for later use.

Preparation of biochar-leachate (BCL) and leached biochar (LBC): According to European Standard BS EN 12457–2:2002 (British Standards Institution 2002), the biochar was mixed in an H_2SO_4 solution (pH = 2.50) at a solid–liquid ratio of 1:10. The solution was placed in a shaker (ZQLY-180S, Shanghai, China) and oscillated at 180 rpm at 28 °C for 24 h. The mixture was centrifuged at 5000 rpm for 5 min, and the supernatant was passed through a 0.45 μm filter membrane to obtain the biochar-leachate with a BC concentration of 100 g L^{-1}. The resulting BCL was stored at 4 °C in a refrigerator protected from light. The solid obtained after centrifugation was the leached biochar (LBC). It was dried at 50 °C and stored for later use.

Preparation of the *A. ferrooxidans* cell suspension: *A. ferrooxidans* LX5 was obtained from the Solid Waste Research Institute, Nanjing Agricultural University, China. The strain was activated three times in 150 mL of modified 9K liquid culture medium and then centrifuged to obtain a 30-fold concentrated *A. ferrooxidans* cell suspension (Dong et al. 2018; Fu et al. 2023; Liao et al. 2009).

2.2 Experimental methods

2.2.1 Effect of biochar and biochar-leachate on the ability of A. ferrooxidans to biooxidize Fe(II)

In a series of Erlenmeyer flasks, 6.67 g of $FeSO_4 \cdot 7H_2O$ was dissolved in ultrapure water. Then, 1 mL of the 30-fold concentrated *A. ferrooxidans* cell suspension was added to the solution. At the same time, 3 mL of 100 g BC L^{-1} biochar-leachate (BCL), 0.3 g of original biochar (BC), and 0.3 g of leached biochar (LBC) were added at a mass ratio of $FeSO_4 \cdot 7H_2O$ to biochar of 20:1, and no biochar or biochar-leachate was used as a blank control (CK). Ultrapure water was added to a total reaction volume of 150 mL, and the initial density of *A. ferrooxidans* in each system was 7.0×10^7 copies mL^{-1}. There were four treatment groups in the experiment, and each treatment was repeated three times. The pH of all the treatment solutions was adjusted to 2.50 ± 0.01 with 2 mol L^{-1} H_2SO_4. The samples were sealed with eight layers of sterilized gauze and placed in a shaker at 180 rpm and oscillated at 28 ℃ until all the Fe(II) in the control was completely oxidized. The pH and Fe(II) oxidation efficiency of the system were measured every 12 h during the study period, and the mineral weight (in terms of dry matter) of each treatment was determined after the end of the culture.

2.2.2 Effect of bacterial density and biochar and biochar-leachate dose on the ability of A. ferrooxidans to biooxidize Fe(II)

$FeSO_4 \cdot 7H_2O$ (6.67 g) was dissolved in ultrapure water. Then, 0.2, 0.4, 0.6, 0.8, or 1.0 mL of the 30-fold concentrated *A. ferrooxidans* cell suspension was added to the solution, and the rest of the procedure was the same as that described in Sect. 2.2.1, with the total reaction volume still 150 mL. The initial densities of *A. ferrooxidans* in each group were 1.4×10^7, 2.8×10^7, 4.2×10^7, 5.6×10^7, and 7.0×10^7 copies mL^{-1}.

Similarly, after dissolving 6.67 g of $FeSO_4 \cdot 7H_2O$ in ultrapure water, BCL, BC, and LBC were added to the solution at mass ratios of $FeSO_4 \cdot 7H_2O$ to biochar of 100:1, 50:1, 20:1, 10:1, and 5:1, respectively, and a blank control (CK) was established. The rest of the procedure was the same as that described in Sect. 2.2.1, with the total reaction volume being 150 mL. Therefore, the initial

density of *A. ferrooxidans* in each group was 7.0×10^7 copies mL^{-1}.

The pH of all the treatment solutions was adjusted to 2.50 ± 0.01 with 2 mol L^{-1} H_2SO_4. The samples were sealed with eight layers of sterilized gauze and placed in a shaker at 180 rpm and oscillated at 28 ℃ for 84 h. The pH and Fe(II) oxidation efficiency of the system were measured every 12 h during this period.

2.2.3 Removal of As(III) and Cd(II) from a simulated AMD system by biochar

$FeSO_4 \cdot 7H_2O$ (6.67 g) was dissolved in 149 mL of ultrapure water and As(III)/Cd(II) solution (both at a concentration of 10 mg L^{-1}), and 1 mL of the 30-fold concentrated *A. ferrooxidans* cell suspension was added to the solution. BC was added according to a mass ratio of $FeSO_4 \cdot 7H_2O$ to biochar of 20:1, while a biochar-free treatment was used as the control. Furthermore, a control treatment used to evaluate As(III)/Cd(II) adsorption to biochar was established. Five treatment groups were used in the experiment, and each treatment was repeated three times. The pH of all the treatment solutions was adjusted to 2.50 ± 0.01 with 2 mol L^{-1} H_2SO_4. The samples were sealed with eight layers of sterilized gauze and placed in a shaker at 180 rpm and oscillated at 28 ℃ for 72 h. The pH, Fe(II) oxidation efficiency, and total As and Cd concentrations of the solution were measured every 12 h.

2.3 Analytical methods

The pH and conductivity of the solution were measured using a pH meter (PHS-3C, Shanghai, China) and a conductivity meter (DDS-11A, Shanghai, China), respectively. The total organic carbon (TOC) content of the solution was determined using a TOC analyzer (multi N/C 3100 TOC, Jena, Germany). The concentrations of major ions (K^+, Ca^{2+}, Na^+, Mg^{2+}, F^-, Cl^-, NO_3^-, etc.) were measured using an ion chromatograph (IC6200, Anhui, China). The Fe(II) concentration was determined using a visible-light spectrophotometer (V-1100D, Shanghai, China) (Liao et al. 2011; Zhu et al. 2013). The concentration of total As was determined using a hydride generation atomic fluorescence spectrometer (AFS-2100, Beijing, China). The concentration of total Cd was determined using a graphite furnace atomic absorption spectrometer (PE 900Z, USA). The organic matter components in the biochar-leachate were analyzed using a three-dimensional excitation-emission matrix (3D EEM) (Chen et al. 2003) and a three-dimensional fluorescence spectrometer (RF-5301PC, Shimadzu, Japan). The organic components in the solution were determined using high-performance liquid chromatography–mass spectrometry (HPLC–MS, Waters 2695 + ZQ2000, USA)
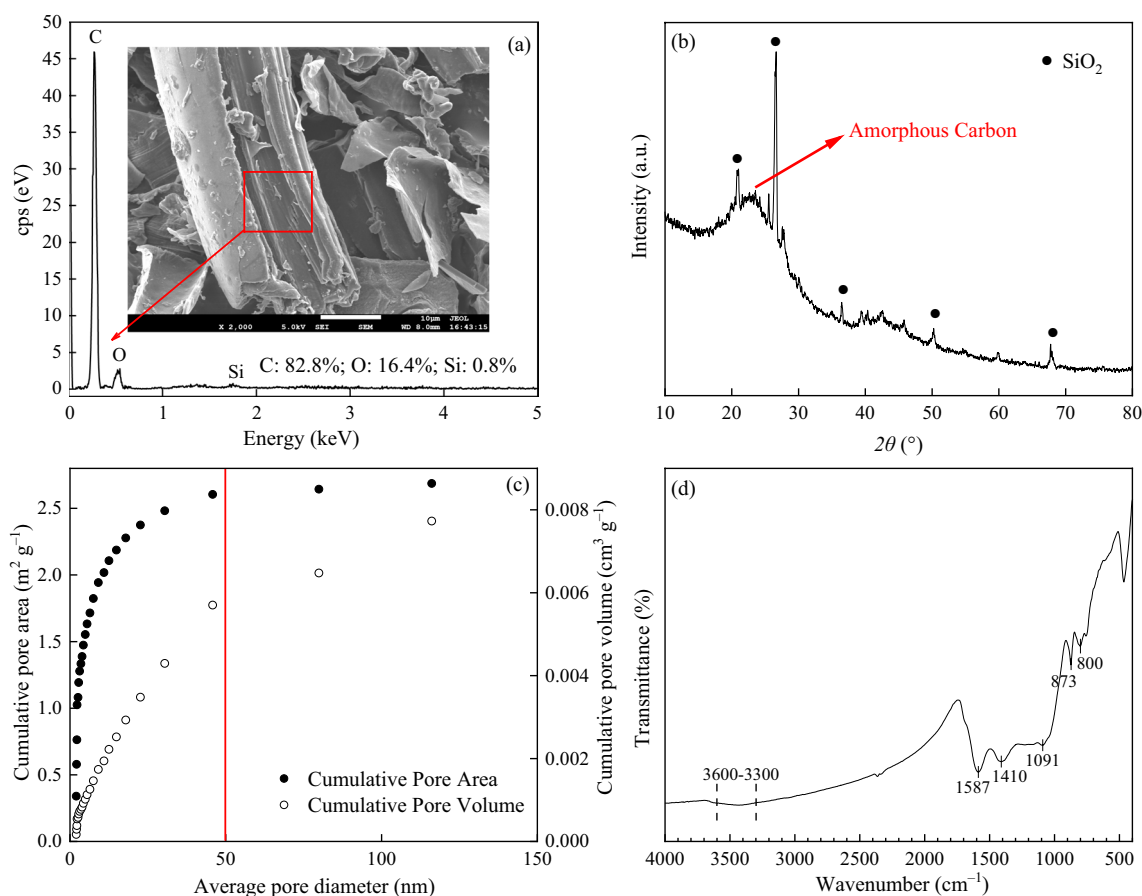
Fig. 1 Characterization of biochar: **a** surface morphology and elemental analysis, **b** X-ray diffraction pattern, **c** pore size distribution, and **d** Fourier transform infrared spectrum

(Yuan et al. 2017). The electrospray-positive ion mode [ESI (+)] and negative ion mode [ESI (−)] were used for testing. Based on methods in previous studies (Fu et al. 2023), the surface morphology and elemental composition of the materials were analyzed using a field emission scanning electron microscope (SEM, JSM-7001F, Japan) with an accelerating voltage of 5.0 kV. Phase analysis of the materials was performed using an X-ray powder diffractometer (XRD, MiniFlex II, Japan) with a Cu Kα X-ray source. The Raman spectra of the materials were determined using a Raman microscope (Renishaw inVia, UK) with an excitation wavelength of 532 nm. The specific surface area and pore size distribution of the materials were determined via an automatic specific surface and pore analyzer (TriStar II 3020, USA). Surface functional groups were identified by a fourier transform infrared spectrometer (FTIR, Tensor 27, Germany). The C_T value and 16S rRNA gene copy number of *A. ferrooxidans* were measured using an RT−qPCR system (ABI 7500, Thermo Scientific, USA) (Escobar et al. 2008; Smith et al. 2006; Sun et al. 2012). DNA was extracted using a rapid DNA

extraction kit (DP336, TIANGEN, China). The test kit used was TB Green™ Premix Ex Taq™ II (Tli RNaseH Plus) (Takara, Code No. RR820A).

2.4 Data and statistical analysis

The raw data obtained from the positive ion [ESI (+)] and negative ion modes [ESI (−)] of the HPLC−MS system were searched against the databases Metlin, MassBank, MoNA, and HMDB, and the results were screened. Substances detected in at least two of three parallel experiments were considered to be present. In this study, IBM SPSS 19.0 was used for statistical analysis and single-factor analysis of variance (ANOVA) for all the data, and Duncan's test was used for significance analysis ($p < 0.05$). The figures were generated using OriginPro 2023b.

3 Results and discussion
3.1 Characterization of biochar and biochar-leachate
3.1.1 Characterization of biochar

The characteristics of the biochar are shown in Fig. 1. The biochar had a smooth surface with a large number

of lamellar, columnar, and massive structures with pores on the surface. The surface elements were dominated by C (82.8%) and contain small amounts of O and Si. Phase analysis revealed peaks at $2\theta = 20.86°$, 26.64°, 36.54°, 50.14°, and 67.74°, confirming the presence of SiO_2 (JCPDS: 46-1045) (Song et al. 2021; Zhang et al. 2019). In addition, a weaker broad peak centered at $2\theta = 23.5°$ appeared in the diffraction pattern. Similar characteristic peaks have been reported in other studies (Mandal et al. 2020; Tan et al. 2023). This might be related to the presence of highly disordered amorphous carbon in the biochar. Raman spectra (Additional file 1: Fig. S1a) showed that biochar had characteristic peaks near both 1360 and 1590 cm^{-1}, corresponding to the D-band and G-band, respectively. The D-band reflects the degree of disorder of the carbon material, while the G-band responds to its degree of graphitization (Yang et al. 2017). The specific surface area of the biochar was 12.8 m^2 g^{-1}. The pore size distribution revealed that the average pore size ranged from 2 to 50 nm, suggesting that mesopores contributed significantly to the specific surface area. A large specific surface area and rich pore structure can provide abundant adsorption sites, which endow biochar with high adsorption capacity.

The types of functional groups on the biochar surface were also analyzed (Fig. 1d). There were three more distinct absorption peaks in the functional group region. A wide absorption peak occurred in the range of 3600–3300 cm^{-1} mainly due to the –OH stretching vibration of hydrogen bonds. The peak at 1587 cm^{-1} may be related to C=C and C=O bending vibrations in the benzene ring or aromatic heterocycles, which are typical functional groups on biochar (Sui et al. 2021; Taheri et al. 2023). The peak at 1410 cm^{-1} corresponds to the stretching vibration of phenolic hydroxyl groups in biochar. In addition, in the fingerprint region, the peak at 1091 cm^{-1} corresponds to the pyran skeleton vibration of C–O–C, and the characteristic absorption peak of Si–O–Si also occurs here (Liu and Fan 2018). The two peaks at 873 and 800 cm^{-1} may be due to the in-plane bending vibrations of C–H in the benzene ring.

3.1.2 Composition analysis of biochar-leachate

Additional file 1: Table S1 lists the basic physicochemical properties and main ion content of the biochar-leachate. The results showed that the biochar-leachate was alkaline (pH = 9.65) and had low total organic carbon (TOC, 86.93 mg L^{-1}) content and a high content of major anions and cations (K$^+$, Ca^{2+}, Mg^{2+}, Cl$^-$, etc.), and the Cl$^-$ content reached 831.85 mg L^{-1}. A comparison revealed that the main components of biochar-leachate were similar to those of the 9 K liquid medium and could provide nutrients for *A. ferrooxidans* growth and reproduction.

Figure 2 shows the results of spectral and chromatographic analysis of the biochar-leachate. Figure 2a shows the Fourier transform infrared spectrum, which was used to analyze the types of functional groups contained in the biochar-leachate. The wide peak in the range of 3600–3200 cm^{-1} corresponds to the stretching vibration of –OH. The peak at 1637 cm^{-1} may be the stretching vibration of C=C and C=O in a benzene or aromatic heterocyclic ring. Weaker narrow peaks appeared at 1383 and 1352 cm^{-1}, possibly indicating the in-plane bending vibration of –OH in alcohols or phenols (Jiao et al. 2019). The peak at 1069 cm^{-1} may be caused by the pyran skeletal vibration of C–O–C (Liu and Fan 2018).

Figure 2b shows the three-dimensional fluorescence spectra of the organic matter contained in the biochar-leachate. According to the classification method shown in Additional file 1: Table S2 (Chen et al. 2003; Li et al. 2018), the fluorescent areas are concentrated in regions III and V, accounting for 17.07% and 68.06%, respectively, of the total area, indicating that the biochar-leachate mainly contained fulvic acid-like and humic acid-like substances. Analysis of their chemical formulae revealed that the carbon numbers of these organics were mainly in the range of C10 and C22, with C16 organics being the most abundant (Fig. 2c). The elements comprising these organics were C, H, O, N, P, S, F, and Cl, which were used to classify the substances (Fig. 2d). Among these, CHNO and CHO were the dominant species, accounting for 47.3% and 22.0%, respectively, of the total species. In addition, based on the ratios of H/C and O/C atoms in the molecular formulae, the substances were classified into lipids, aliphatic proteins, unsaturated hydrocarbons, and lignins, and Van Krevelen diagrams were constructed (Fig. 2e) (Yuan et al. 2017; Zhong et al. 2022). The diagrams show that unsaturated hydrocarbons and lignin substances were predominant in the dissolved organic matter (DOM) in the biochar-leachate. These results are similar to those of other studies. The material composition of the DOM in the biochar was correlated with the pyrolysis temperature. At higher pyrolysis temperatures, the content of fulvic acid-like and humic acid-like substances in the DOM was relatively high (Yang et al. 2020b). In addition, other studies have shown that the content of proteins and lipids decreases as the pyrolysis temperature increases. At higher pyrolysis temperatures (500 °C), the DOM in biochar is dominated by lignin and aromatic compounds (Huang et al. 2021).

3.2 Effect of biochar and biochar-leachate on the ability of *A. ferrooxidans* to biooxidize Fe(II)

3.2.1 Process of Fe(II) bio-oxidation by A. ferrooxidans

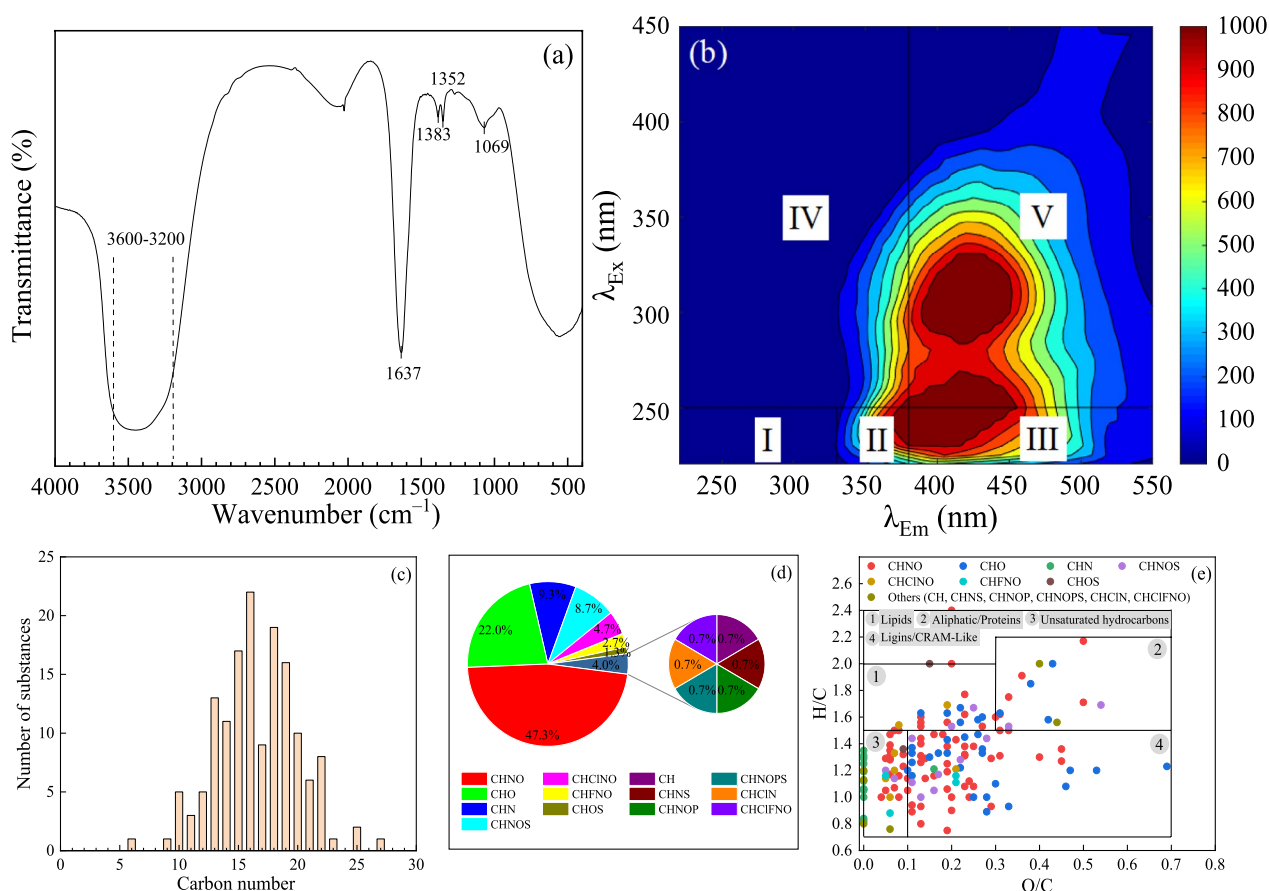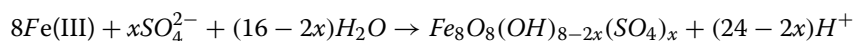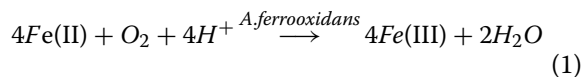The pH and Fe(II) oxidation efficiency curves changed during the culture of *A. ferrooxidans* (Fig. 3). The pH in

Fig. 2 Analysis of the organic matter composition in the biochar-leachate: **a** Fourier transform infrared spectrum, **b** three-dimensional fluorescence spectra, **c** organic matter carbon number distribution, **d** element composition classification and proportion, and **d** Van Krevelen diagram

each treatment showed a trend of first increasing and then decreasing and fell to ~ 2.0 after 72 h. This occurred because the *A. ferrooxidans* growth process included two stages: (1) the oxidation of Fe(II) to consume protons and (2) the hydrolysis of Fe(III) to produce protons (Eqs. (1)–(2)). The pH of the system increased slightly with the addition of BC and BCL compared to that of the control treatment. This is because the additives were alkaline and had a buffering effect on the acid–base environment of the system.

$$4Fe(\text{II}) + O_2 + 4H^+ \xrightarrow{A.ferrooxidans} 4Fe(\text{III}) + 2H_2O \tag{1}$$

$$8Fe(\text{III}) + xSO_4^{2-} + (16 - 2x)H_2O \rightarrow Fe_8O_8(OH)_{8-2x}(SO_4)_x + (24 - 2x)H^+ \tag{2}$$

The results showed that the addition of BCL promoted Fe(II) oxidation to some extent, accelerating this process by approximately two percentage points

compared with that of the control. This might have occurred because the anions and cations (K^+, Ca^{2+}, Mg^{2+}, Cl^-, etc.) in the BCL could be utilized by *A. ferrooxidans* as nutrients, promoting the growth and reproduction of the bacteria and accelerating the process of Fe(II) oxidation. In addition, studies have shown that low-molecular-weight organic acids contained in DOM have toxic effects on *A. ferrooxidans* (Ren et al. 2009). However, in the present study, composition analysis of the biochar-leachate showed that it contained a low TOC content and that the DOM was dominated by unsaturated hydrocarbons and lignin substances, with little or no low-molecular-

weight organic acids. This is because the composition of DOM in biochar is related to the pyrolytic preparation temperature. The biochar obtained from high-temperature pyrolysis had a lower content of
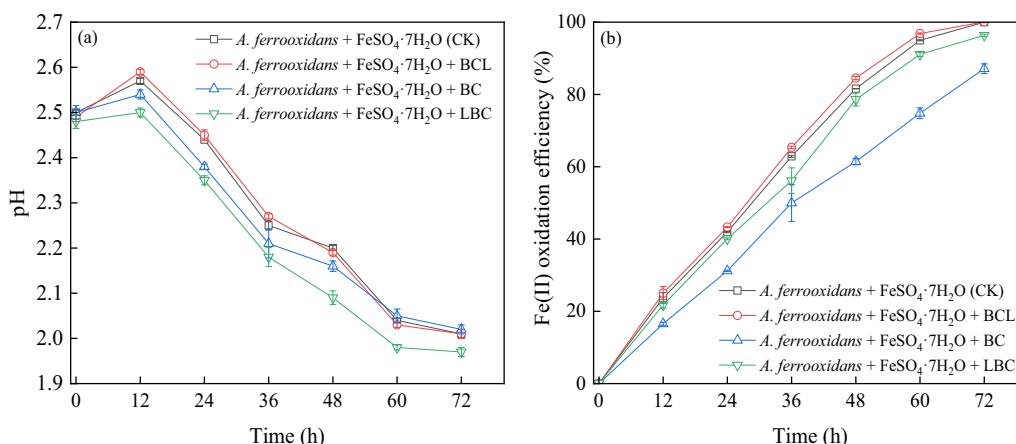
Fig. 3 pH (**a**) and Fe(II) oxidation efficiency (**b**) during the culture of *A. ferrooxidans* [Both BC and LBC were added at a mass ratio of FeSO$_4$·7H$_2$O to biochar of 20:1, and 100 g BC L^{-1} BCL was added at the same ratio]

low-molecular-weight organic acids in the DOM and a higher content of humus-like substances (Bian et al. 2019). In this study, biochar was prepared by pyrolysis at 500 °C, and the composition of the DOM conformed to the abovementioned pattern; therefore, the biochar had weak toxic effect on *A. ferrooxidans*.

However, the addition of BC and LBC inhibited this process. This might have occurred because the biochar added to the system adsorbed a fraction of the *A. ferrooxidans*, while more schwertmannite was attached to the biochar surface and wrapped around the *A. ferrooxidans*, blocking the pore channels and preventing the normal transfer of substrates, O$_2$, and CO$_2$, which resulted in weakened activity and reduced biooxidation capacity (Li et al. 2017; Yang et al. 2020a).

Furthermore, to determine whether the leaching time of biochar influences its properties, affecting the growth of *A. ferrooxidans*, we subjected the biochar to leaching for up to 10 days and replicated this part of the experiment (see Additional file 1: Table S1 and Fig. S2). The results showed that the trend in pH was the same for each treatment in both sets of experiments. The Fe(II) oxidation efficiency again showed an increasing trend, and the addition of BCL also had a slight promoting effect. Consequently, the biochar leaching time had little effect on the physicochemical properties or the effect of the biochar-leachate on Fe(II) oxidation.

3.2.2 Products of Fe(II) biooxidation by A. ferrooxidans

Figure 4 and Table 1 show data for the characterization of the products obtained from Fe(II) biooxidation by *A. ferrooxidans* in the above experiments. Analysis of the XRD patterns (Fig. 4a, b) and comparison with a standard card (JCPDS: 47-1775) confirmed that the characteristic peaks at *2θ* values of 35.16° and 61.34° in the control

could be attributed to schwertmannite (Schoepfer and Burton 2021). The surface of the mineral had an obvious needle-like burr structure and a spherical agglomerated structure. Schwertmannite was also obtained after BCL treatment. However, while its surface morphology and phase did not change significantly, the specific surface area decreased, and the Fe/S ratio increased. Notably, the addition of BCL improved the mineral yield by 8%, which has positive implications for the practical production and application of schwertmannite.

The addition of biochar resulted in decreased mineral production because the biooxidation of Fe(II) by *A. ferrooxidans* was hindered. However, the specific surface area of the product was greater than that of schwertmannite because of the larger amount of schwertmannite attached to the biochar surface. This can be seen in Fig. 4e, f. In addition, the analysis of the XRD patterns showed that the products obtained after the addition of biochar not only showed the characteristic peaks of schwertmannite and biochar but also the peaks of jarosite (JCPDS: 22-0827) at *2θ* values of 17.41°, 28.96°, 45.86°, and 49.93°, which indicated that the introduction of biochar affected the biooxidation of Fe(II) by *A. ferrooxidans*, and new substances were generated. This finding aligns with our previous findings (Fu et al. 2023). Additionally, Raman data (Additional file 1: Fig. S1b) indicated an increase in the intensity ratio of the D-band to the G-band (I$_D$/I$_G$) after the composite of schwertmannite and biochar. This ratio is often used to assess the degree of disorder and defects in carbon materials. This suggested that the complexation of the schwertmannite increased the degree of disorder in the biochar and formed more defective sites (Li et al. 2022). Meanwhile, the I$_D$/I$_G$ of Sch-LBC (0.795) was higher than that of Sch-BC (0.751). This might be due to the fact that
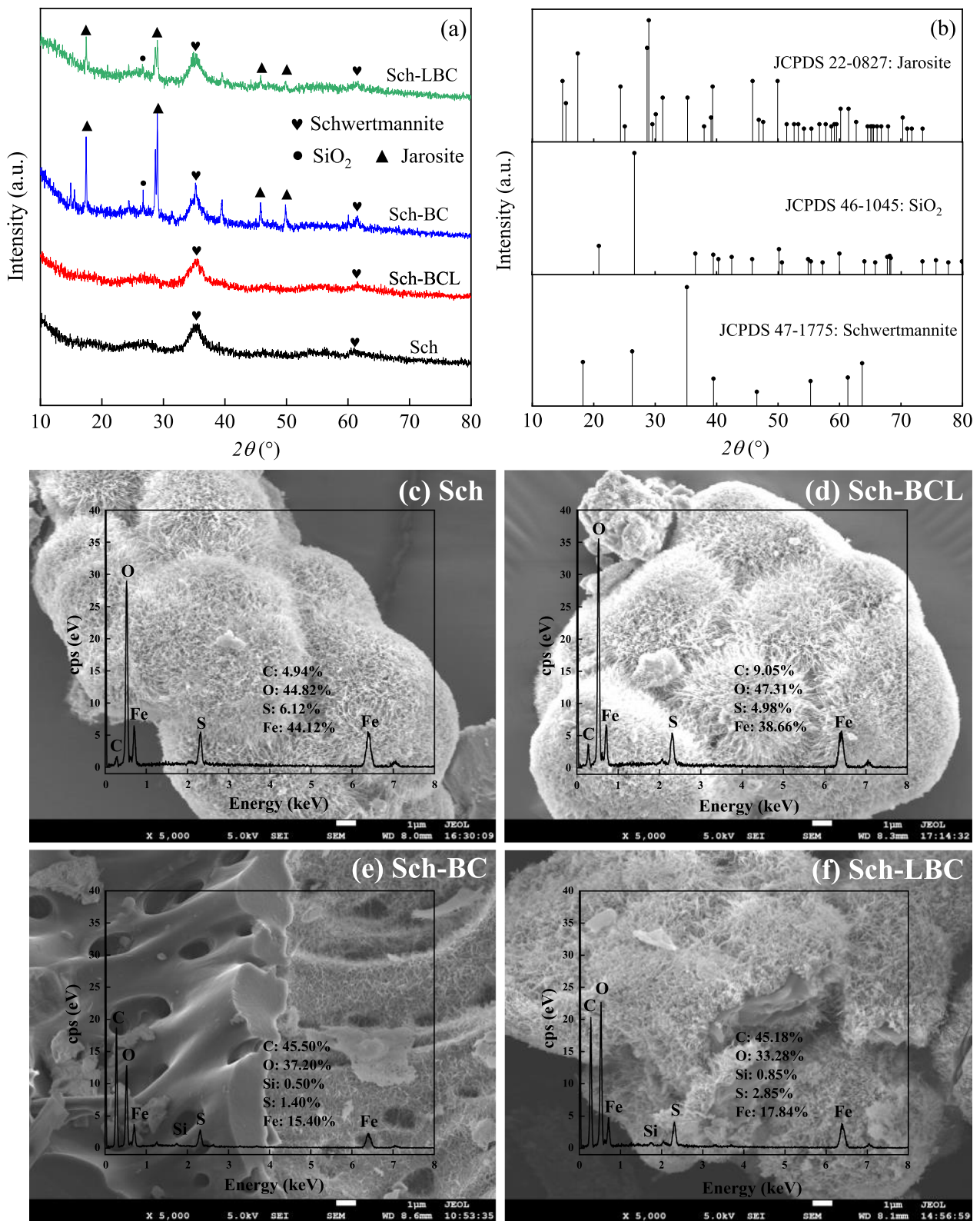
Fig. 4 Characterization analysis of the products obtained from each treatment: **a**, **b** X-ray diffraction pattern and standard card and **c–f** surface morphology and elemental analysis

Table 1 Mineral yield, specific surface area, and Fe/S of each treatment

Treatment	Product abbreviation	Minerals yield (g L^{-1})	Specific surface area (m^2 g^{-1})	Fe/S
A. ferrooxidans + FeSO$_4$·7H$_2$O (CK)	Sch	3.37	2.28	4.15
A. ferrooxidans + FeSO$_4$·7H$_2$O + BCL	Sch-BCL	3.65	2.11	4.44
A. ferrooxidans + FeSO$_4$·7H$_2$O + BC	Sch-BC	3.01	9.58	4.07
A. ferrooxidans + FeSO$_4$·7H$_2$O + LBC	Sch-LBC	3.28	9.72	4.03

acid leaching disrupted the graphitized structure in the biochar material and produced a large amount of amorphous carbon structure.

We also conducted adsorption experiments on heavy metals and metalloids using these materials (Fu et al. 2023) and found that the removal of As(III) by a schwertmannite-biochar composite was approximately 1.4 times greater than that by schwertmannite alone. The alkali-modified composites also effectively removed Cd(II). These findings have significant implications for the removal of As(III) and Cd(II) from industrial wastewater.

3.3 Effect of bacterial density on the ability of *A. ferrooxidans* to biooxidize Fe(II)

The effect of bacterial density on the ability of *A. ferrooxidans* to biooxidize Fe(II) in the biochar system is shown in Fig. 5. Overall, the pH of the solution in each treatment initially increased and then decreased. As the density of *A. ferrooxidans* increased during the early stages

of culture, the increase in pH became less obvious. This resulted in a rapid decrease in the pH of the system, leading to a lower pH at the endpoint. This is because the pH change in the system was regulated by both proton consumption during Fe(II) oxidation and proton production during Fe(III) hydrolysis. When the density of *A. ferrooxidans* was low, the quantity of protons consumed by Fe(II) oxidation was greater than that produced by Fe(III) hydrolysis during the early stages of culture. The endpoint pH of each system with BCL and LBC was slightly lower than that of the control, whereas the endpoint pH of each system with BC was slightly higher than that of the control. This finding is similar to the pattern observed in previous experiments.

The Fe(II) oxidation efficiency in all treatment systems showed an increasing trend with increasing *A. ferrooxidans* density. When c(*A. ferrooxidans*) = 1.4 × 10^7 copies mL^{-1} and m(FeSO$_4$·7H$_2$O):m(biochar) = 20:1, after 84 h of culture, the Fe(II) oxidation efficiency was
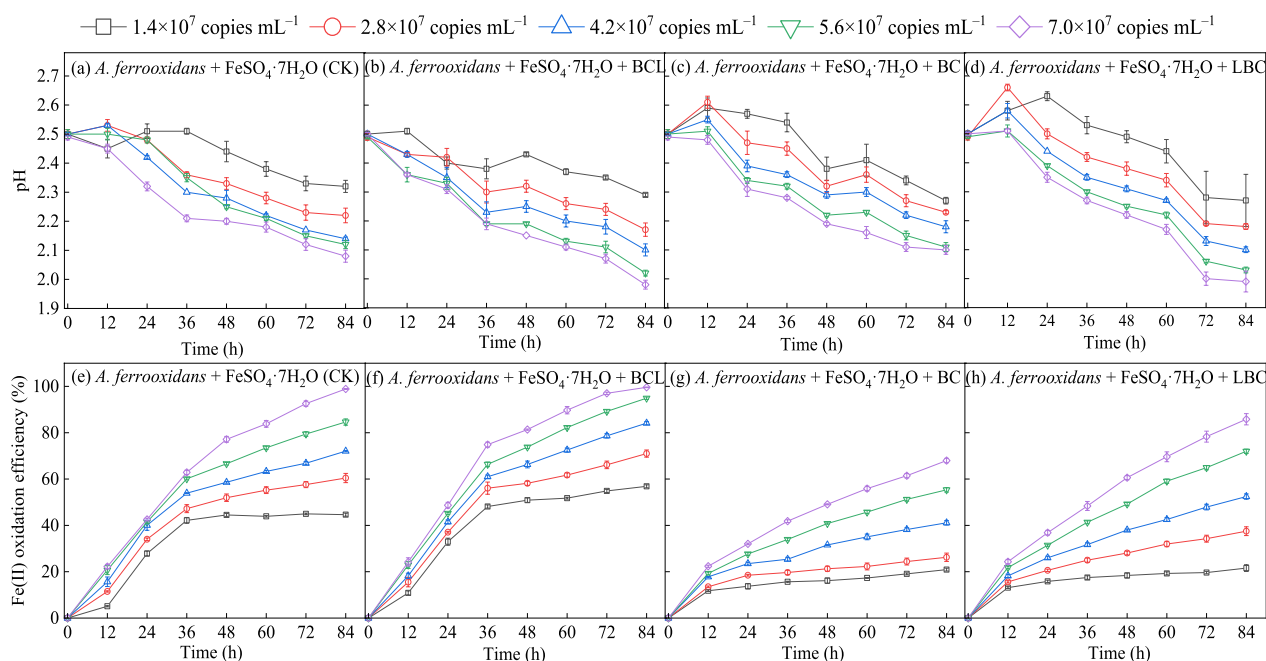

Fig. 5 Effect of bacterial density on the ability of *A. ferrooxidans* to biooxidize Fe(II) in the biochar system [Both BC and LBC were added at a mass ratio of FeSO$_4$·7H$_2$O to biochar of 20:1, and 100 g BC L^{-1} BCL was added at the same ratio; **a–d** pH change, **e–h** Fe(II) oxidation efficiency]

only ~20% for the treatments with BC and LBC. When $c(A.\ ferrooxidans) = 7.0 \times 10^7$ copies mL^{-1} and m(FeSO$_4$·7H$_2$O):m(biochar) = 20:1, after 84 h of culture, the Fe(II) oxidation efficiencies were 98.89% and 99.59% for the CK treatment and treatment with BCL, respectively, while efficiencies of 67.99% and 85.82% were obtained for the treatments with BC and LBC, respectively. During the culture process, the Fe(II) oxidation efficiency in each system with BCL was slightly higher than that in the control, and the trend in the rate was similar in both groups, with the oxidation rate being faster in the first 36 h, and then gradually slowing down thereafter. In contrast, the Fe(II) oxidation efficiency in the two groups treated with biochar was significantly lower than that in the control group, and rapid oxidation of Fe(II) occurred in the first 12 h. This might have occurred because the introduction of biochar had some effect on the growth of *A. ferrooxidans*, leading to weaker activity in the latter stages; therefore, Fe(II) oxidation slowed.

3.4 Effect of biochar and biochar-leachate dose on the ability of *A. ferrooxidans* to biooxidize Fe(II)

The effects of biochar and biochar-leachate dose on the ability of *A. ferrooxidans* to biooxidize Fe(II) are shown in Fig. 6. The pH in each treatment group increased at first and then decreased. After 84 h of culture, the Fe(II) oxidation efficiency of the control was 98.70%. The Fe(II) oxidation efficiency gradually increased in all the treatments. There was no significant difference between the treatments in the BCL-treated groups and the control group. However, as the biochar dose was increased, the inhibitory effect of biochar on the Fe(II) biooxidation process of *A. ferrooxidans* became stronger. The inhibitory effect was most significant in the BC-added treatment. The treatment containing BC at a mass ratio of FeSO$_4$·7H$_2$O to biochar of 5:1 had an Fe(II) oxidation efficiency of only 26% after 84 h of culture. The addition of small amounts of LBC had a weak inhibitory effect on this process. The trend in Fe(II) oxidation was not significantly different from that of the control treatment in which LBC was added according to a mass ratio
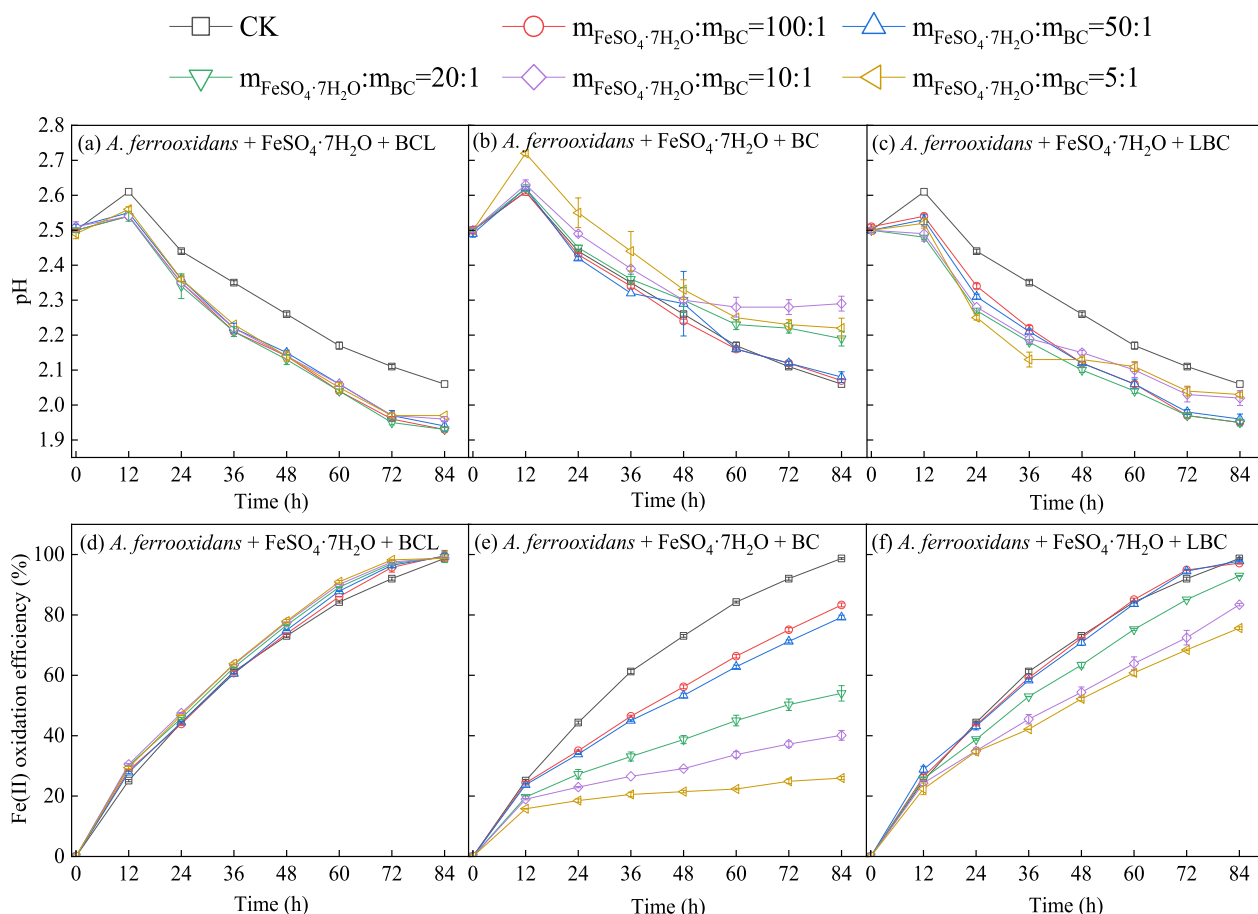

Fig. 6 Effect of biochar and biochar-leachate dose on the ability of *A. ferrooxidans* to biooxidize Fe(II) [Both BC and LBC were added at a fixed ratio, and 100 g BC L^{-1} BCL was added at the same ratio; **a–c** pH curve, **d–f** Fe(II) oxidation efficiency curve]

of FeSO$_4$·7H$_2$O to biochar of 100:1. Even with the addition of LBC at a mass ratio of 5:1, the Fe(II) oxidation efficiency reached a value greater than 75% after 84 h of culture.

To confirm the adsorption of biochar on *A. ferrooxidans*, we added 1.0 mL of the 30-fold concentrated *A. ferro*oxidans cell suspension to 149 mL of ultrapure water (c(*A. ferrooxidans*) = 7.0×10^7 copies mL^{-1}) and added BC according to a mass ratio of FeSO$_4$·7H$_2$O to biochar of 20:1. The bacteria were subsequently cultured for 84 h under the same experimental conditions. At the end of incubation, the ratio of *A. ferrooxidans* in the solid phase to liquid phase was approximately 17:1. The results showed that biochar strongly adsorbed *A. ferrooxidans*. This finding is similar to that of previous studies (Yang et al. 2020a). Therefore, in this study, the addition of BC according to the mass ratio of FeSO$_4$·7H$_2$O to biochar

of 5:1 had no significant effect on the Fe(II) oxidation efficiency after 12 h of reaction. This indicated that a large fraction of the *A. ferrooxidans* in the system was adsorbed and immobilized by the biochar. The content of free *A. ferrooxidans* in the liquid phase was even lower than the initial content, and this fraction could not react effectively with Fe(II); thus, the Fe(II) oxidation efficiency decreased.

3.5 Removal of As(III) and Cd(II) from a simulated AMD system by biochar

Based on the above experiments, we investigated the adsorption of As(III) and Cd(II) on biochar in a simulated AMD system, and the results are shown in Fig. 7. The pH of the *A. ferrooxidans* biooxidation system first increased and then decreased. Under As(III) and Cd(II) cocontamination, the oxidation efficiency of Fe(II) was slightly
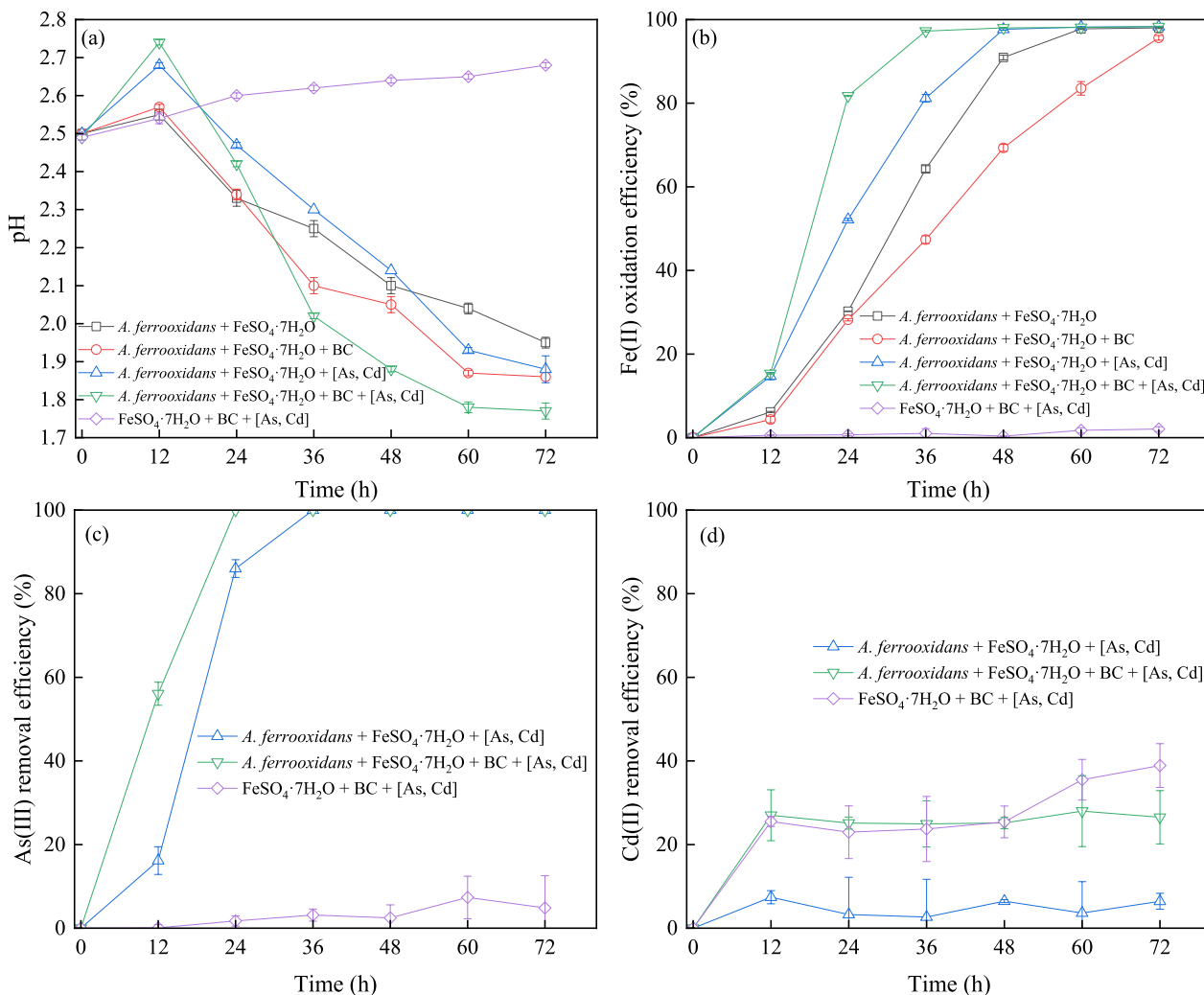

Fig. 7 Experimental results of coprecipitation and adsorption of As(III) and Cd(II) in water [Initial As(III) and Cd(II) concentrations: 10 mg L^{-1}; BC was added according to a mass ratio of FeSO$_4$·7H$_2$O to biochar of 20:1]

higher in each system, and oxidation was complete after 48 h. Treatment with biochar resulted in a Fe(II) oxidation rate of 80% at 24 h after the start of the reaction. At this point, schwertmannite had begun to be generated. As shown in Fig. 7c, the biochar in the control group (without *A. ferrooxidans*) exhibited poor adsorption of As(III), with less than 10% removal. In the simulated AMD system, As(III) was adsorbed within 24 h after the start of the reaction, for a removal efficiency of approximately 100%. Previous studies have shown that there are usually two methods for As removal with schwertmannite in practical AMD systems. One is that As and Fe are directly involved in the formation of the crystal structure of schwertmannite through coprecipitation; the other is that schwertmannite adsorbs As in solution through electrostatic attraction or ion-exchange (Park et al. 2016; Zhang et al. 2016). However, under acidic conditions, As(III) in solution mainly exists in the form of electrically neutral H_3AsO_3 molecules (Additional file 1: Fig. S3a), making electrostatic attraction and ion-exchange more difficult. Therefore, in this study, the removal of As(III) might have occurred due to coprecipitation with the schwertmannite generated by the biooxidation of *A. ferrooxidans*. Additionally, previous studies showed that lower As/Fe molar ratios favor the introduction of As into the structure of schwertmannite in acidic systems, while higher As/Fe molar ratios favor the formation of amorphous Fe(III)-As(III)/As(V) coprecipitates (Maillot et al. 2013). These studies supported our conclusions.

As shown in Fig. 7 d, the removal of Cd(II) by biochar in the control group (without *A. ferrooxidans*) was approximately 40%. However, in the simulated AMD system, the biochar adsorbed Cd(II) only during the first 12 h of the reaction and then adsorption equilibrium was reached, with a removal efficiency of 26.53%. These results indicated that the adsorption capacity of biochar for Cd(II) was limited in a strongly acidic environment (pH ~ 2.5). This was because the adsorption of Cd(II) by biochar was carried out mainly by electrostatic attraction (Tan et al. 2022). However, under acidic conditions, Cd(II) in solution mainly exists in the form of Cd^{2+} (Additional file 1: Fig. S3b). Moreover, the biochar surface adsorbs positive charges, making electrostatic attraction difficult. Considering the limitations to the adsorption performance of biochar in acidic environments, it is necessary to refine this technique in subsequent studies to improve the Cd(II) adsorption efficiency. Overall, biochar could remove Cd(II) in the AMD system, but the removal rate was limited. The schwertmannite generated in the reaction covered the surface of the biochar, which not only immobilized the already adsorbed Cd(II) but also promoted excellent removal of As(III). This finding suggests a novel approach for the removal of heavy metals and metalloids from AMD.

4 Conclusions

Biochar-leachate had a promoting effect on the production of schwertmannite from the biooxidation of Fe(II) by *A. ferrooxidans*, whereas biochar had an inhibitory effect on this process. The inhibition by biochar was more pronounced when the density of *A. ferrooxidans* in the system was low or when the biochar dose was high. This study confirmed that this inhibition might be due to the adsorption of a large fraction of the *A. ferrooxidans* present by the biochar in the system, as well as the attachment of schwertmannite to the surface of the biochar, which blocked pore channels and prevented the ready transfer of substrates, O_2, and CO_2, resulting in weakened bacterial activity and reduced reproductive capacity. In addition, the introduction of biochar led to a change in the Fe(II) biooxidation products of *A. ferrooxidans* from schwertmannite to jarosite, and the specific surface area increased after biochar addition. Coprecipitation experiments of As(III) and Cd(II) showed that As(III) was completely adsorbed by the schwertmannite generated during the reaction within 24 h. However, the biochar only adsorbed Cd(II) within the first 12 h of the reaction, and the adsorption of Cd(II) by biochar in the AMD system needs to be further investigated. Overall, this study extends the research on environmental microorganisms to the field of environmental functional materials. In this study, heavy metals and metalloids were simultaneously adsorbed using biochar produced from agricultural waste and schwertmannite generated from an AMD system, realizing the goal of "treating waste with waste" and providing an innovative solution for the removal of As(III) and Cd(II) from AMD.

Supplementary Information

The online version contains supplementary material available at https://doi.org/10.1007/s42773-024-00324-3.

Additional file 1: Table S1. Basic physicochemical properties and main ion contents of biochar-leachate. **Table S2.** Three-dimensional fluorescence spectrogram partitioning. **Figure S1.** Raman spectra of materials: (a) original biochar, (b) the products obtained from each treatment. **Figure S2.** pH (a) and Fe(II) oxidation efficiency (b) during the culture of *A. ferrooxidans*. [Both BC and LBC were added at a mass ratio of $FeSO_4 \cdot 7H_2O$ to biochar of 20:1, and 100 g BC L^{-1} BCL (leaching for 10 d) was added at the same ratio.] **Figure S3.** Equilibrium distribution of As(III) (a) and Cd(II) (b) species in solutions with different pH.

Data availability
All data generated or analyzed during this study are included in manuscript and supplementary material.

Declarations

Competing interests
The authors have no relevant financial or non-financial interests to disclose.

Author details
[1]College of Resource and Environment, Shanxi Agricultural University, Taigu 030801, China. [2]Graduate School of Science and Engineering, Saitama University, Saitama 338-8570, Japan. [3]College of Resources and Environmental Sciences, Nanjing Agricultural University, Nanjing 210095, China. [4]Department of Geography and Environmental Science, University of Reading, Reading RG6 6AB, UK.

References

Anawar HM, Akter F, Solaiman ZM, Strezov V (2015) Biochar: an emerging panacea for remediation of soil contaminants from mining, industry and sewage wastes. Pedosphere 25:654–665. https://doi.org/10.1016/s1002-0160(15)30046-1

Bian R, Joseph S, Shi W, Li L, Taherymoosavi S, Pan G (2019) Biochar DOM for plant promotion but not residual biochar for metal immobilization depended on pyrolysis temperature. Sci Total Environ 662:571–580. https://doi.org/10.1016/j.scitotenv.2019.01.224

British Standards Institution BS (2002) Characterisation of waste – Leaching – Compliance test for leaching of granular waste materials and sludges –. Part 2: One stage batch test at a liquid to solid ratio of 10 L/kg for materials with particle size below 4 mm (without or with size reduction). BS EN 12457-2:2002, London, UK.

Chen W, Westerhoff P, Leenheer JA, Booksh K (2003) Fluorescence excitation-emission matrix regional integration to quantify spectra for dissolved organic matter. Environ Sci Technol 37:5701–5710. https://doi.org/10.1021/es034354c

Chen G, Ye Y, Yao N, Hu N, Zhang J, Huang Y (2021) A critical review of prevention, treatment, reuse, and resource recovery from acid mine drainage. J Clean Prod 329:129666. https://doi.org/10.1016/j.jclepro.2021.129666

Chi T, Zuo J, Liu F (2017) Performance and mechanism for cadmium and lead adsorption from water and soil by corn straw biochar. Front Environ Sci Eng 11:15. https://doi.org/10.1007/s11783-017-0921-y

Colmer AR, Hinkle ME (1947) The role of microorganisms in acid mine drainage: a preliminary report. Science 106:253–256. https://doi.org/10.1126/science.106.2751.253

Dong Y, Liu F, Qiao X, Zhou L, Bi W (2018) Effects of acid mine drainage on calcareous soil characteristics and *Lolium perenne* L. germination. Int J Environ Res Public Health 15:2742. https://doi.org/10.3390/ijerph15122742

Dong Y, Chong S, Lin H (2022) Enhanced effect of biochar on leaching vanadium and copper from stone coal tailings by *Thiobacillus ferrooxidans*. Environ Sci Pollut Res 29:20398–20408. https://doi.org/10.1007/s11356-021-17259-y

Du T, Bogush A, Masek O, Purton S, Campos LC (2022) Algae, biochar and bacteria for acid mine drainage (AMD) remediation: a review. Chemosphere 304:135284. https://doi.org/10.1016/j.chemosphere.2022.135284

Duan C, Ma T, Wang J, Zhou Y (2020) Removal of heavy metals from aqueous solution using carbon-based adsorbents: a review. J Water Process Eng 37:101339. https://doi.org/10.1016/j.jwpe.2020.101339

Escobar B, Bustos K, Morales G, Salazar O (2008) Rapid and specific detection of *Acidithiobacillus ferrooxidans* and *Leptospirillum ferrooxidans* by PCR. Hydrometallurgy 92:102–106. https://doi.org/10.1016/j.hydromet.2008.01.012

Fu P, Wang X, Shi J, Zhou L, Hou Q, Wang W, Tian Y, Qin J, Bi W, Liu F (2023) Enhanced removal of As(III) and Cd(II) from wastewater by alkali-modified Schwertmannite@Biochar. Environ Technol Inno 31:103197. https://doi.org/10.1016/j.eti.2023.103197

Huang M, Li Z, Wen J, Ding X, Zhou M, Cai C, Shen F (2021) Molecular insights into the effects of pyrolysis temperature on composition and copper binding properties of biochar-derived dissolved organic matter. J Hazard Mater 410:124537. https://doi.org/10.1016/j.jhazmat.2020.124537

Islam MS, Kwak JH, Nzediegwu C, Wang S, Palansuriya K, Kwon EE, Naeth MA, El-Din MG, Ok YS, Chang SX (2021) Biochar heavy metal removal in aqueous solution depends on feedstock type and pyrolysis purging gas. Environ Pollut 281:117094. https://doi.org/10.1016/j.envpol.2021.117094

Jiao D, Xie Z, Wan Q, Qu M (2019) Reduced irreversible capacities of graphene oxide-based anodes used for lithium ion batteries via alkali treatment. J Energy Chem 37:73–81. https://doi.org/10.1016/j.jechem.2018.11.018

Jiao Y, Zhang C, Su P, Tang Y, Huang Z, Ma T (2023) A review of acid mine drainage: formation mechanism, treatment technology, typical engineering cases and resource utilization. Process Saf Environ 170:1240–1260. https://doi.org/10.1016/j.psep.2022.12.083

Li H, Dong X, da Silva EB, de Oliveira LM, Chen Y, Ma LQ (2017) Mechanisms of metal sorption by biochars: biochar characteristics and modifications. Chemosphere 178:466–478. https://doi.org/10.1016/j.chemosphere.2017.03.072

Li G, Khan S, Ibrahim M, Sun TR, Tang JF, Cotner JB, Xu YY (2018) Biochars induced modification of dissolved organic matter (DOM) in soil and its impact on mobility and bioaccumulation of arsenic and cadmium. J Hazard Mater 348:100–108. https://doi.org/10.1016/j.jhazmat.2018.01.031

Li T, Zhu P, Wang D, Zhang Z, Zhou L (2022) Efficient utilization of the electron energy of antibiotics to accelerate Fe(III)/Fe(II) cycle in heterogeneous Fenton reaction induced by bamboo biochar/schwertmannite. Environ Res 209:112830. https://doi.org/10.1016/j.envres.2022.112830

Liao Y, Zhou L, Liang J, Xiong H (2009) Biosynthesis of schwertmannite by *Acidithiobacillus ferrooxidans* cell suspensions under different pH condition. Mat Sci Eng C 29:211–215. https://doi.org/10.1016/j.msec.2008.06.011

Liao Y, Liang J, Zhou L (2011) Adsorptive removal of As(III) by biogenic schwertmannite from simulated As-contaminated groundwater. Chemosphere 83:295–301. https://doi.org/10.1016/j.chemosphere.2010.12.060

Liu L, Fan S (2018) Removal of cadmium in aqueous solution using wheat straw biochar: effect of minerals and mechanism. Environ Sci Pollut Res 25:8688–8700. https://doi.org/10.1007/s11356-017-1189-2

Liu F, Lei Y, Shi J, Zhou L, Wu Z, Dong Y, Bi W (2020) Effect of microbial nutrients supply on coal bio-desulfurization. J Hazard Mater 384:121324. https://doi.org/10.1016/j.jhazmat.2019.121324

Maillot F, Morin G, Juillot F, Bruneel O, Casiot C, Ona-Nguema G, Wang Y, Lebrun S, Aubry E, Vlaic G, Brown GE (2013) Structure and reactivity of As(III)- and As(V)-rich schwertmannites and amorphous ferric arsenate sulfate from the Carnoulès acid mine drainage, France: comparison with biotic and abiotic model compounds and implications for As remediation. Geochim Cosmochim Ac 104:310–329. https://doi.org/10.1016/j.gca.2012.11.016

Mandal S, Pu S, Wang X, Ma H, Bai Y (2020) Hierarchical porous structured polysulfide supported nZVI/biochar and efficient immobilization of selenium in the soil. Sci Total Environ 708:134831. https://doi.org/10.1016/j.scitotenv.2019.134831

Masindi V, Foteinis S, Renforth P, Ndiritu J, Maree JP, Tekere M, Chatzisymeon E (2022) Challenges and avenues for acid mine drainage treatment, beneficiation, and valorisation in circular economy: a review. Ecol Eng 183:106740. https://doi.org/10.1016/j.ecoleng.2022.106740

Moinier D, Byrne D, Amouric A, Bonnefoy V (2017) The global redox responding RegB/RegA signal transduction system regulates the genes involved in ferrous iron and inorganic sulfur compound oxidation of the acidophilic *Acidithiobacillus ferrooxidans*. Front Microbiol 8:1277. https://doi.org/10.3389/fmicb.2017.01277

Park JH, Han YS, Ahn JS (2016) Comparison of arsenic co-precipitation and adsorption by iron minerals and the mechanism of arsenic natural attenuation in a mine stream. Water Res 106:295–303. https://doi.org/10.1016/j.watres.2016.10.006

Park I, Tabelin CB, Jeon S, Li X, Seno K, Ito M, Hiroyoshi N (2019) A review of recent strategies for acid mine drainage prevention and mine tailings recycling. Chemosphere 219:588–606. https://doi.org/10.1016/j.chemosphere.2018.11.053

Pierre Louis AM, Yu H, Shumlas SL, Van Aken B, Schoonen MAA, Strongin DR (2015) Effect of phospholipid on pyrite oxidation and microbial communities under simulated acid mine drainage (AMD) conditions. Environ Sci Technol 49:7701–7708. https://doi.org/10.1021/es505374g

Qiu B, Tao X, Wang H, Li W, Ding X, Chu H (2021) Biochar as a low-cost adsorbent for aqueous heavy metal removal: a review. J Anal Appl Pyrol 155:105081. https://doi.org/10.1016/j.jaap.2021.105081

Ren WX, Li PJ, Zheng L, Fan SX, Verhozina VA (2009) Effects of dissolved low molecular weight organic acids on oxidation of ferrous iron by *Acidithiobacillus ferrooxidans*. J Hazard Mater 162:17–22. https://doi.org/10.1016/j.jhazmat.2008.05.005

Schoepfer VA, Burton ED (2021) Schwertmannite: a review of its occurrence, formation, structure, stability and interactions with oxyanions. Earth-Sci Rev 221:103811. https://doi.org/10.1016/j.earscirev.2021.103811

Smith CJ, Nedwell DB, Dong LF, Osborn AM (2006) Evaluation of quantitative polymerase chain reaction-based approaches for determining gene copy and gene transcript numbers in environmental samples. Environ Microbiol 8:804–815. https://doi.org/10.1111/j.1462-2920.2005.00963.x

Song J, Huang Z, Gamal El-Din M (2021) Adsorption of metals in oil sands process water by a biochar/iron oxide composite: Influence of the composite structure and surface functional groups. Chem Eng J 421:129937. https://doi.org/10.1016/j.cej.2021.129937

Sui L, Tang C, Du Q, Zhao Y, Cheng K, Yang F (2021) Preparation and characterization of boron-doped corn straw biochar: Fe(II) removal equilibrium and kinetics. J Environ Sci 106:116–123. https://doi.org/10.1016/j.jes.2021.01.001

Sun LX, Zhang X, Tan WS, Zhu ML (2012) Effect of agitation intensity on the biooxidation process of refractory gold ores by *Acidithiobacillus ferrooxidans*. Hydrometallurgy 127–128:99–103. https://doi.org/10.1016/j.hydromet.2012.07.007

Taheri MR, Astaraei AR, Lakzian A, Emami H (2023) The role of biochar and sulfur-modified biochar on soil water content, biochemical properties and millet crop under saline-sodic and calcareous soil. Plant Soil 183:1–16. https://doi.org/10.1007/s11104-023-05912-z

Tan Y, Wan X, Ni X, Wang L, Zhou T, Sun H, Wang N, Yin X (2022) Efficient removal of Cd(II) from aqueous solution by chitosan modified kiwi branch biochar. Chemosphere 289:133251. https://doi.org/10.1016/j.chemosphere.2021.133251

Tan X, Liu J, Liu M, Zhang Y, Liu Q, Duan G, Cui J, Lin A (2023) Arsenic removal and stabilization behavior of schwertmannite@BC (Sch@BC) in contaminated dual media (water/soil): via sulfate exchange and chemical complexation. Environ Pollut 325:121431. https://doi.org/10.1016/j.envpol.2023.121431

Tu Z, Wu Q, He H, Zhou S, Liu J, He H, Liu C, Dang Z, Reinfelder JR (2022) Reduction of acid mine drainage by passivation of pyrite surfaces: a review. Sci Total Environ 832:155116. https://doi.org/10.1016/j.scitotenv.2022.155116

Valente T, Grande JA, de la Torre ML, Gomes P, Santisteban M, Borrego J, Sequeira Braga MA (2015) Mineralogy and geochemistry of a clogged mining reservoir affected by historical acid mine drainage in an abandoned mining area. J Geochem Explor 157:66–76. https://doi.org/10.1016/j.gexplo.2015.05.016

Wang Z, Xu Y, Zhang Z, Zhang Y (2020) Review: acid mine drainage (AMD) in abandoned coal mines of Shanxi, China. Water 13:8. https://doi.org/10.3390/w13010008

Xi H, Min F, Yao Z, Zhang J (2022) Facile fabrication of dolomite-doped biochar/bentonite for effective removal of phosphate from complex wastewaters. Front Environ Sci Eng 17:71. https://doi.org/10.1007/s11783-023-1671-7

Yang H, Xie P, Ni L, Flower RJ (2012) Pollution in the Yangtze. Science 337:410. https://doi.org/10.1126/science.337.6093.410-a

Yang H, Flower RJ, Thompson JR (2013) Sustaining China's water resources. Science 339:141. https://doi.org/10.1126/science.339.6116.141-b

Yang H, Huang X, Thompson JR (2015) Biochar: pros must outweigh cons. Nature 518:483. https://doi.org/10.1038/518483f

Yang F, Sun L, Xie W, Jiang Q, Gao Y, Zhang W, Zhang Y (2017) Nitrogen-functionalization biochars derived from wheat straws via molten salt synthesis: an efficient adsorbent for atrazine removal. Sci Total Environ 607–608:1391–1399. https://doi.org/10.1016/j.scitotenv.2017.07.020

Yang B, Luo W, Wang X, Yu S, Gan M, Wang J, Liu X, Qiu G (2020a) The use of biochar for controlling acid mine drainage through the inhibition of chalcopyrite biodissolution. Sci Total Environ 737:139485. https://doi.org/10.1016/j.scitotenv.2020.139485

Yang F, Zhang Q, Jian H, Wang C, Xing B, Sun H, Hao Y (2020b) Effect of biochar-derived dissolved organic matter on adsorption of sulfamethoxazole and chloramphenicol. J Hazard Mater 396:122598. https://doi.org/10.1016/j.jhazmat.2020.122598

Yuan Z, He C, Shi Q, Xu C, Li Z, Wang C, Zhao H, Ni J (2017) Molecular insights into the transformation of dissolved organic matter in landfill leachate concentrate during biodegradation and coagulation processes using ESI FT-ICR MS. Environ Sci Technol 51:8110–8118. https://doi.org/10.1021/acs.est.7b02194

Yue T, Yang Y, Li L, Su M, Wang M, Liao Y, Jia L, Chen S (2023) Application prospect of anaerobic reduction pathways in *Acidithiobacillus ferrooxidans* for mine tailings disposal: a review. Minerals 13:1192. https://doi.org/10.3390/min13091192

Zhan Y, Yang M, Zhang S, Zhao D, Duan J, Wang W, Yan L (2019) Iron and sulfur oxidation pathways of *Acidithiobacillus ferrooxidans*. World J Microb Biot 35:60. https://doi.org/10.1007/s11274-019-2632-y

Zhang SL, Jia SY, Yu B, Liu Y, Wu SH, Han X (2016) Sulfidization of As(V)-containing schwertmannite and its impact on arsenic mobilization. Chem Geol 420:270–279. https://doi.org/10.1016/j.chemgeo.2015.11.020

Zhang L, Tang S, He F, Liu Y, Mao W, Guan Y (2019) Highly efficient and selective capture of heavy metals by poly (acrylic acid) grafted chitosan and biochar composite for wastewater treatment. Chem Eng J 378:122215. https://doi.org/10.1016/j.cej.2019.122215

Zhao Y, Chen P, Nan W, Zhi D, Liu R, Li H (2015) The use of (5Z)-4-bromo-5-(bromomethylene)-2(5H)-furanone for controlling acid mine drainage through the inhibition of *Acidithiobacillus ferrooxidans* biofilm formation. Bioresource Technol 186:52–57. https://doi.org/10.1016/j.biortech.2015.02.017

Zhong Q, Zhang Z, Fu Q, Yu J, Liao X, Zhao J, He D (2022) Molecular level insights into HO$^{\bullet}$ and Cl$_2^{\bullet-}$-mediated transformation of dissolved organic matter in landfill leachate concentrates during the Fenton process. Chem Eng J 446:137062. https://doi.org/10.1016/j.cej.2022.137062

Zhu J, Gan M, Zhang D, Hu Y, Chai L (2013) The nature of schwertmannite and jarosite mediated by two strains of *Acidithiobacillus ferrooxidans* with different ferrous oxidation ability. Mat Sci Eng C 33:2679–2685. https://doi.org/10.1016/j.msec.2013.02.026